Theoretical analysis of the graphitization of a nanodiamond

2007 J. Phys.: Condens. Matter 19 386215

(http://iopscience.iop.org/0953-8984/19/38/386215)

IOP PUBLISHING JOURNAL OF PHYSICS: CONDENSED MATTER

J. Phys.: Condens. Matter **19** (2007) 386215 (10pp) doi:10.1088/0953-8984/19/38/386215

Theoretical analysis of the graphitization of a nanodiamond

S Joon Kwon[1] **and Jae-Gwan Park**

Nano Science and Technology Division, Korea Institute of Science and Technology (KIST), PO Box 131, Cheongryang, Seoul, 130-650, Korea

E-mail: cheme@kist.re.kr (S J Kwon)

Received 22 June 2007
Published 31 August 2007
Online at stacks.iop.org/JPhysCM/19/386215

Abstract

We report on a theoretical analysis of the graphitization of a nanosize diamond (nanodiamond) in the metastable state. A nanodiamond annealed at a relatively lower temperature suffers morphological transition into a nanodiamond–graphite core–shell structure. Thermodynamic stability analysis of the nanodiamond showed that the phase diagram (relationship between the annealing temperature and radius) of the nanodiamond–graphite has three regimes: smaller nanodiamond, nanodiamond–graphite, and larger nanodiamond. These regimes of nanodiamond–graphite are due to an additional phase boundary from finding the maximum size of the nanodiamond which can be graphitized. In the theoretical analysis, the most probable and the maximum volume fractions of graphite in the nanodiamond were 0.76 and 0.84 respectively, which were independent of the annealing temperature and the initial radius of the nanodiamond. Therefore, the nanodiamond is not completely transformed into graphite by simple annealing at relatively lower process temperature and pressure. The highest graphitization probability decreased with increasing annealing temperature. Raman spectra for the F_{2g} vibration mode of nanodiamond were also calculated, and we found that the variation in properties of the spectral line was strongly dependent on the graphitization temperature and the initial size of the nanodiamond.

1. Introduction

Nanosize diamond (nanodiamond) has attracted considerable interest due to its important properties for industrial application. These properties include not only conventional diamond characteristics such as high thermal conductivity, high hardness, low coefficient of friction, etc, but also specific characteristics of optical and magnetic properties [1, 2]. The nanodiamond can be transformed into graphite by simple annealing or high explosive detonation at a relatively

[1] Author to whom any correspondence should be addressed.

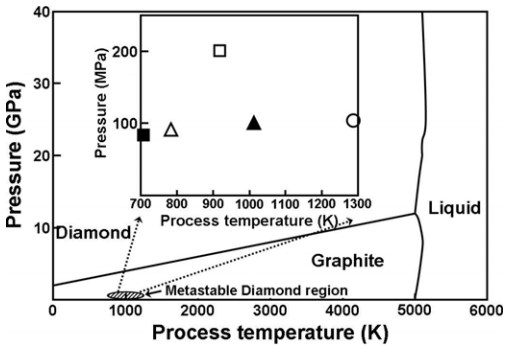

Figure 1. Phase diagram of carbon represented by the process pressure–process temperature relationship. The oblique lined ellipsoidal region indicates the metastable phase responsible for the nucleation of diamond during the duration of the graphitization. The inset is an enlarged view of the metastable phase of the diamond, and the symbols in the inset (■, △, □, ▲, ○) indicate the experimental data obtained from the references [23, 24, 21, 20, 22], respectively.

low temperature and atmospheric pressure due to the high value of the surface area to volume ratio [3–8]. This graphitization results in the variation in the surface-dependent physical properties of the nanodiamond such as magnetoresistivity, surface free energy, electrical resistivity, etc. To make use of the nanodiamond in variety of engineering applications, perspective understanding of the graphitization of the nanodiamond is required. Some research groups concentrated on the systematic research on the graphitization of the nanodiamond involving Raman spectroscopy analysis [4, 6, 9–14], kinetics analysis [7, 15], graphitization mechanism based on the interatomic potential analysis [16], and thermodynamic analysis on the stability of the nanodiamond annealed at relatively low temperature and at atmospheric pressure [17]. The analysis on the size-dependent stability of the nanodiamond during the graphitization enabled us to find the size-dependent phase diagram of the nanodiamond and graphite expressed by the relationship between the annealing temperature and the size of the diamond [17], and critical conditions for the formation of the stable and metastable phases of the nanodiamond could be predicted along with the calculation of the critical size of the nucleation of the synthesis of the nanodiamond [18].

In this study, a theoretical analysis elucidating the existence of an additional phase diagram boundary between the nanodiamond and graphite is presented. The presented analysis is mainly based on the analysis of the thermodynamic stability of the graphitization accompanied by the modified Laplace pressure affected by the nanosize curvature of the diamond in the metastable state [17, 18]. Along with the finding of the additional phase boundary, the analysis shows that the most probable and the maximum volume fractions of graphite in the nanodiamond have constant values, without reference to the annealing temperature and the size of the nanodiamond. Calculated Raman spectra of the nanodiamond graphitized were also provided for the detailed study of the thermodynamics of the graphitization of a nanodiamond.

2. Stability analysis of the graphitization of a nanodiamond

2.1. Determination of a threshold critical size of a nanodiamond for graphitization

As was experimentally reported [2, 4, 5, 7, 17], graphitization occurs at the surface of the nanodiamond of initial radius of r. According to the temperature–pressure phase diagram of carbon [18, 19] shown in figure 1, the nanodiamond is in the metastable state in the region

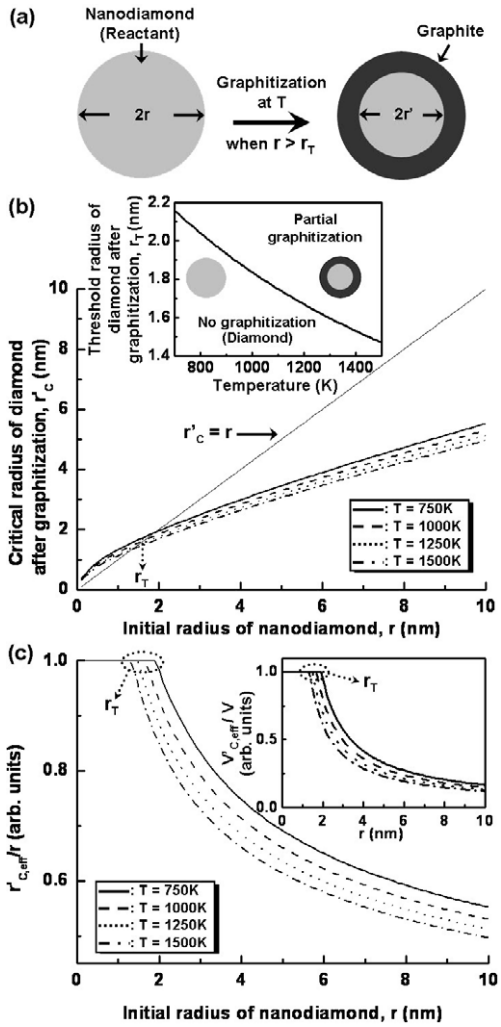

Figure 2. (a) Schematic illustration of the graphitization of a nanodiamond with r resulting in nanodiamond–graphite core–shell structure (core radius of r') at a constant annealing temperature T. (b) Theoretical relationship between r and r'_{C} with differing T. Note that $r'_{\mathrm{C}} > r$ when $r < r_{\mathrm{T}}$. The inset shows the relationship between r_{T} and T. (c) Ratio between r and $r'_{\mathrm{C,eff}}$ with differing T. The inset shows the relationship $V'_{\mathrm{eff}}(= 4\pi r'^{3}_{\mathrm{C,eff}}/3)$ to $V(= 4\pi r^3/3)$ ratio and r with differing T.

defined by the process temperature range of 713–1273 K and the process pressure range of 81–200 MPa [20–24], as is the case in the context of the nucleation process of the nanodiamond derived from gas phase during the duration of phase transition. Under the same scheme as the nucleation process from gas phase, we can think that there is a nucleation stage accompanying a very short existence of a liquid phase for the phase transition of the metastable nanodiamond to graphite. Since the size is small enough, the surface tension in the capillary effect considered in the Laplace–Young equation plays an important role in determining the thermodynamic stability of the nanodiamond. The nanodiamond studied in the present work is in this metastable region, and therefore, the phase transition of the nanodiamond differs from that of the solid phase diamond. Schematic graphitization of the nanodiamond is shown in figure 2(a). If the

graphitization is an energetically favourable process, the free energy of the nanodiamond coated with graphite (core–shell structure of diamond–graphite), ΔG_g, should be lower than that of the initial nanodiamond, ΔG_d. The free energy difference, $\Delta G = \Delta G_g - \Delta G_d$, at the annealing temperature T can be expressed as

$$\Delta G = \Delta G_g - \Delta G_d = 4\pi r^2(\gamma_g - \gamma_d) + \frac{4\pi \Delta V_m}{3V_{mg}}(r^3 - r'^3)\left(A - P - \frac{2\gamma_d}{r'}\right), \quad (1)$$

where r' is the radius of the residual core diamond after the graphitization (refer to figure 2(a)), A is the pressure of the phase equilibrium line in the bulk state of the graphite and diamond, which can be written as $A = 2.01\times10^6 T + 2.02\times10^9$ (Pa), V_{mg} is the molar volume of graphite ($V_{mg} = 5.187 \times 10^{-6}$ m^3 mol^{-1}), ΔV_m is the molar volume difference between diamond ($V_{md} = 3.417 \times 10^{-6}$ m^3 mol^{-1}) and graphite, P is the reaction pressure that is assumed to be atmospheric pressure, γ_g is the surface free energy of graphite ($\gamma_g = 0.55$ J m^{-2}), and γ_d is the surface free energy of diamond ($\gamma_d = 3.7$ J m^{-2}) [17]. Experimental data for the surface energies of the materials relate to the bulk phase. For the sake of simplicity, in equation (1), a sphere-like morphology was assumed [6, 7] for the shape of the nanodiamond. While in general the real shape of the nanodiamond has been reported to be polyhedral [2] involving polyhedral edges and apices, the sphere-like shape assumed here is enough to capture the critical thermodynamic nature of the nanodiamond. It should be noted that $2\gamma_d/r'$ is the nanosize-induced interior pressure of the residual diamond given by the Laplace–Young equation [17, 18]. On the basis of classical thermodynamics, ΔG is minimized with respect to r' for the graphitization and the critical radius of the residual diamond, r'_C, satisfies the following equation:

$$r'^3_C(3Ar'_C - 4\gamma_d) = 2\gamma_d r^3. \quad (2)$$

Shown in figure 2(b) is the relationship between r and r'_C for various annealing temperatures. As is apparent from these plots, r'_C increases with increasing r, and the lower the temperature, the lower the volume fraction of graphite in the nanodiamond. Interestingly, $r'_C > r$ in the case of a relatively small diamond. When $r'_C > r$, the nanodiamond cannot be graphitized at the given temperature. For a nanodiamond satisfying the condition $r > r'_C$, isotropic graphitization occurs on its surface. This size-dependent behaviour of the graphitization of the nanodiamond indicates the existence of a threshold critical radius for the graphitization, r_T when $r = r'_C$, which determines whether the graphitization of the nanodiamond is possible or not. In other words, the effective critical radius of the residual nanodiamond after the graphitization, $r'_{C,eff}$, is equal to r when $r < r_T$ and is equal to r'_C when $r > r_T$. The behaviour of r_T as a function of T, $r_T = 2\gamma_d/A$, is shown in the inset of figure 2(b). An increase in the annealing temperature leads to a decrease in r_T and, interestingly, this behaviour of r_T is exactly consistent with the previous analysis [17]. As was shown in figure 2(c), the value of $r'_{C,eff}/r$ decreases with increasing r in the case where the nanodiamond has a value of r larger than r_T, and so does the ratio of the effective volume of the nanodiamond after the graphitization to the initial volume of the nanodiamond ($r'^3_{C,eff}/r^3$) (refer to the inset of figure 2(c)). These behaviours of $r'_{C,eff}/r$ and $r'^3_{C,eff}/r^3$ indicate that the graphitization is more enhanced for a larger nanodiamond than for a smaller one.

Shown in figure 3(a) is the relationship between ΔG when $r' = r'_C$ (ΔG_C) and r for various annealing temperatures. In these curves, there are two kinds of characteristic radii determining the behaviour of the graphitization of the nanodiamond. The first one is the critical radius of the nanodiamond, r_C, for the minimum value of ΔG_C at a given temperature for which the graphitization of the nanodiamond is most probable. As the inset of figure 3(a) (solid curve) shows, an increase in T leads to a decrease in r_C. Additionally, the value of ΔG_C when $r = r_C$

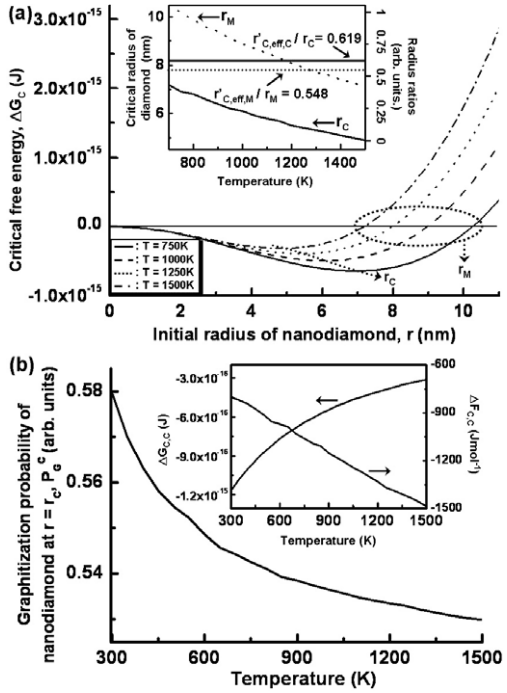

Figure 3. (a) Relationship between ΔG_C and r with differing T. Shown in the inset (left axis) are the relationships between T and two kinds of characteristic radius of the nanodiamond: r_C (solid curve) and r_M (dashed curve). Shown on the right axis of the inset are the relationships between T and the radius ratios between $r'_{C,eff}$ when $r = r_C$ ($r'_{C,eff,C}$) and r_C (solid line), and between $r'_{C,eff}$ when $r = r_M$ ($r'_{C,eff,M}$) and r_M (dashed line). Note that these ratios are constant such that $r'_{C,eff,C}/r_C = 0.619$ and $r'_{C,eff,M}/r_M = 0.548$ respectively, independently of T and r. (b) Relationship between P_G^C and T. Shown in the inset are the relationships between ΔG_C when $r = r_C$ ($\Delta G_{C,C}$)and T, and between $\Delta F_{C,C}$ and T.

($\Delta G_{C,C}$) increases with increasing T. The effective critical radius of the residual nanodiamond at $r = r_C$, $r'_{C,eff,C}$, can be calculated using equations (2) and (3):

$$2r_C(\gamma_g - \gamma_d) + \frac{\Delta V_m}{V_{mg}}\left[3Ar_C^3 - \frac{6\gamma_d r_C^2}{r'_{C,eff,C}} + \left(\frac{2\gamma_d r_C^3}{r'^2_{C,eff,C}} + 4\gamma_d r'_{C,eff,C} - 3Ar'^2_{C,eff,C}\right)\left(\frac{\partial r'_{C,eff,C}}{\partial r}\right)\right] = 0. \quad (3)$$

Then, the ratio between $r'_{C,eff,C}$ and r_C satisfies a relationship of $\alpha(r'_{C,eff,C}/r_C)^4 + (r'_{C,eff,C}/r_C)^3 - 1 = 0$, where $\alpha = \frac{3(\gamma_d - \gamma_g)V_{mg}}{\Delta V_m \gamma_d}$, and the calculated value of $r'_{C,eff,C}/r_C$ is equal to 0.619, independently of the annealing temperature and r, as shown in the inset of figure 3(a) (solid line). This constant value of $r'_{C,eff,C}/r_C$ means that the most probable graphitization of the nanodiamond corresponds to the volume fraction of graphite in the nanodiamond, $1 - (r'_{C,eff,C}/r_C)^3 \sim 0.762$, at any annealing temperature and for any value of r.

2.2. Determination of the maximum allowed size of the nanodiamond for the graphitization

The second characteristic radius is the maximum allowed radius of the nanodiamond which can be graphitized, r_M (when $\Delta G_C = 0$). The theoretical curves for ΔG_C and the inset curve

in figure 3(a) (dashed curve) show that r_M decreases with increasing T. At a relatively high annealing temperature, the largest nanodiamond which can be graphitized is relatively small. Considering the monotonically decreasing behaviour of $r'_{C,eff}/r$ with respect to r (refer to figure 2(c)), the maximum volume fraction of graphite in the nanodiamond $(1-(r'_{C,eff,M}/r_M)^3$, where $r'_{C,eff,M}$ is the effective critical radius of the residual nanodiamond when $r = r_M$) corresponds to a diamond with a critical radius of $r = r_M$, which can be obtained using equations (2) and (4).

$$r_M^2(\gamma_g - \gamma_d) + \frac{\Delta V_m}{3V_{mg}}(r_M^3 - r'^3_{C,eff,M})\left(A - \frac{2\gamma_d}{r'_{C,eff,M}}\right) = 0. \tag{4}$$

Then, the ratio of $r'_{C,eff,M}$ to r_C satisfies the relationship of $(r'_{C,eff,M}/r_C)^3+\beta(r'_{C,eff,M}/r_C)^2-1 = 0$, where $\beta = (3\alpha/2)^{1/2}$, and the calculated value of $r'_{C,eff,M}/r_C$ is equal to 0.548 (the smallest value of $r'_{C,eff}/r$), independently of the annealing temperature and r, as was shown in the inset of figure 3(a) (dashed line). This constant value of $r'_{C,eff,M}/r_C$ means that the graphitization of the largest nanodiamond which can be graphitized corresponds to the maximum volume fraction of graphite in the nanodiamond, $1-(r'_{C,eff,M}/r_C)^3 \sim 0.835$, at any given annealing temperature and for any value of r. This also means that the nanodiamond is not completely transformed into graphite irrespective of the annealing temperature at atmospheric pressure. Interestingly, this theoretical conclusion seems to disagree with recent experimental results reported by Osipov *et al* in which the complete transition of the nanodiamond of 4–5 nm in size to graphite after sufficient annealing time was observed [2]. However, the annealing temperature used in their experiment (∼1873 K) was far above the range of the metastable diamond region shown in figure 1. Moreover, there were no Raman spectra data for the graphitized nanodiamonds less than 5 nm. According to the phonon-confinement model [4, 13], we found that the linewidth of the Raman shift for the F_{2g} mode vibration of a nanodiamond with a size of 5 nm considerably increases from 34.17 cm^{-1} (for a nanodiamond with $2r = 5.0$ nm prior to the graphitization at 1873 K) to 64.38 cm^{-1} (for graphite–diamond core–shell structure with $2r_{C,eff} = 3.7$ nm after graphitization at 1873 K). Therefore, variation in Raman spectra corresponding to the F_{2g} mode vibration given by annealing at 1873 K would exhibit a very low and broad peak at the wavenumber around 1331 cm^{-1} [4, 13]. By examining the Raman spectra obtained under high resolution with shorter excitation wavelength (or with higher detection sensitivity), the existence of core–shell structure of a graphite–nanodiamond predicted in the present study can be confirmed only if the annealing temperature 1873 K can be involved in the metastable diamond region. As regards the discrepancy between the theoretical analysis and experimental results reported in the literature, more detailed and expanded studies on the effects of several factors such as the kinetics, shape, crystallinity, and chemistry of more realistic nanodiamonds on the thermodynamic stability of the nanodiamond could be incorporated to complement and improve the theoretical conclusion solely depending on the thermodynamics. Expanded and detailed studies involving these factors will be done in the near future.

Figure 3(b) shows the relationship between the graphitization probability of the nanodiamond when $r = r_C$ (P_G^C) and the annealing temperature. In order to calculate P_G^C, ΔG_C when $r = r_C$ ($\Delta G_{C,C}$) was normalized to $\Delta F_{C,C}$, which is the molar free energy for the graphitization, $\Delta F_{C,C} = \frac{3\Delta G_{C,C}V_{mg}}{4\pi(r_C^3 - r'^3_{C,eff,C})}$ (J mol^{-1}). As was shown in the inset of figure 3(b), $\Delta G_{C,C}$ increases, while $\Delta F_{C,C}$ decreases, with increasing T. Due to this decreasing behaviour of $\Delta F_{C,C}$, $P_G^C = \exp(\frac{-\Delta F_{C,C}}{RT})/[1+\exp(\frac{-\Delta F_{C,C}}{RT})]$ decreases with increasing T, as is apparent from figure 3(b). However, the decrease in P_G^C given by an increase in T is quite small compared to the increase in T. This behaviour of P_G^C contradicts the previous analysis of

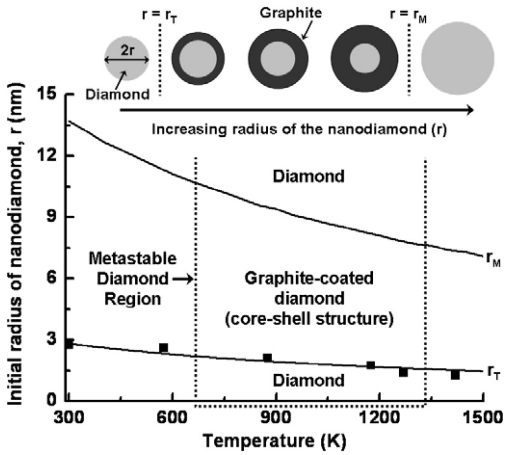

Figure 4. Phase diagram of the nanodiamond–graphite at atmospheric pressure expressed by the relationship between r and T. Square symbols indicate experimental data obtained from the literature [17]. The upper inset is a schematic illustration showing the change of the volume fraction of graphite in the nanodiamond at the given temperature with increasing r with the maximum fraction of 0.84. The dashed region indicates the temperature range responsible for the metastable phase of the nanodiamond.

the graphitization probability in [17], in which P_G increases with increasing T and the increase in the value of P_G is quite pronounced after some threshold annealing temperature is reached for a given r. As is apparent from figure 3(b), no distinctive threshold annealing temperature for a drastic change in the value of P_G^C was found. It is also noteworthy that finding r_M as a function of T means that the phase diagram of the nanodiamond–graphite should be modified to elucidate the size- and annealing temperature-dependent behaviour of the graphitization of the nanodiamond.

As shown in figure 4, the allowed region for the existence of a stable nanodiamond–graphite (isotropic core–shell structure not homogeneous graphite) is restricted to the area between the two phase diagram lines: r_T and r_M. For instance, a nanodiamond with an initial radius larger than 8.39 nm (r_T) or smaller than 1.61 nm (r_M) cannot be transformed into a stable graphite–nanodiamond structure (or does not suffer the surface graphitization) at $T = 1275$ K. At a process temperature higher than $T = 1275$ K which is the maximum temperature of the experimentally reported metastable region of the nanodiamond, however, the limitations in the size of the nanodiamond for the graphitization (r_T and r_M) would not hold when the nanodiamond does not suffer the metastable nucleation process (out of the metastable diamond region). Increasing the process temperature and pressure out of the metastable diamond region will restrict the phase diagram which allows finding a stable region of the nanodiamond under annealing at a constant temperature. Experimentally, one of the phase diagram lines between the nanodiamond and the core–shell diamond–graphite (this line corresponds to r_T) was observed [17], as shown in figure 4. Brodka *et al* also reported that the diamond–graphite core–shell structure forms when the annealing temperature is raised from 1200 to 1500 K [25]. This experimental result is matched well with our analysis, since 3 nm diameter nanodiamond is not transformed into a core–shell structure at 1200 K ($r_T = 1.67$ nm) while it is transformed into a core–shell structure at 1500 K ($r_T = 1.47$ nm). Obraztsova *et al* also provided experimental data showing that the 5 nm diameter diamond annealed at 1100 K might suffer a surface graphitization based on the Raman spectra showing strong evidence of the existence

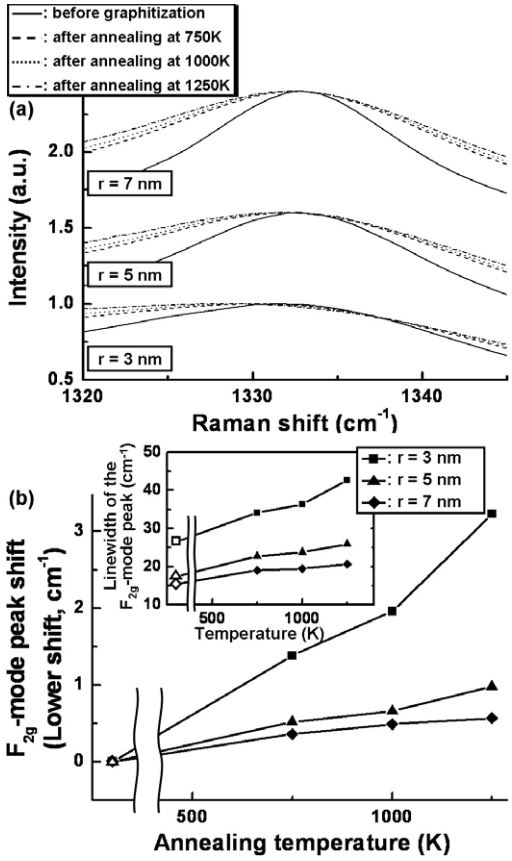

Figure 5. (a) Calculated Raman spectra of nanodiamond in the specified range of wavenumber corresponding to the F_{2g} vibration mode of diamond with differing T and r. (b) Peak shift corresponding to the F_{2g} vibration mode toward lower wavenumber as a function of T. The inset shows the variation in the linewidth of the peak corresponding to the F_{2g} vibration mode as a function of T. Dark symbols are for the graphitized nanodiamond and open symbols are for the nanodiamond prior to the graphitization.

of graphite such as D and G bands which are intrinsic Raman peaks of graphite [26]. This experimental result also provides strong evidence of the existence of the phase diagram line corresponding to r_T. A recent theoretical study on the thermodynamic stability of nanocarbon given by Jiang and Chen [27] seems to give a phase diagram line different to that corresponding to r_T; however the referred to experimental data used for the comparison in the study of Jiang and Chen do not bolster their conclusion, since the compared data showed strong evidence of the existence of graphite after annealing of a 5.5 nm diameter nanodiamond at 1073 K [4]. As regards the phase boundary given by r_M, Gamarnik showed that nanodiamond less than a critical size is more stable than graphite in the numerical calculation [28], and Alexenskii *et al* reported that nanodiamond is more stable than graphite (i.e. diamond smaller than 4.3 nm at 1200 K was observed to be more stable than graphite) in their experimental study of the phase transition of an ultradisperse diamond cluster [6]. Another phase boundary line responsible for r_M has not been experimentally observed or verified by the numerical calculations, and the existence of this line is expected to be confirmed by experiments in the near future.

2.3. Raman spectra of the graphitized nanodiamond

The graphitization of the nanodiamond can be examined using several experimental methods. Here, we give calculated Raman spectra of the nanodiamond during the duration of graphitization in order to give substantial information on the nanodiamond graphitized for the experimental studies on the nanodiamond. In the event of having Raman spectra of a nanosize diamond, the phonon-confinement model can be employed in which the line shape of the spectra is described by superimposition of a group of Lorentzian line shapes [4, 12, 13, 29]. And the intensity of the Raman spectra $I(\omega)$ as a function of the Raman shift (frequency) ω is expressed as follows [4, 13, 29]:

$$I(\omega) = \int_0^1 \frac{4\pi q \exp(-q^2 L^2/4)\,\mathrm{d}q}{[\omega - 1193.75 - 139.25\cos(q\pi)]^2 + [(2.990 + \frac{520}{L})/2]^2}, \tag{5}$$

where q is the wavevector confined in a spherical Brillouin zone in units of $(2\pi/a)$, and the size of the crystal L is in units of $a = 3.567$ Å which is the lattice constant of diamond [29].

Figure 5(a) shows Raman spectra calculated by using equation (5) showing the F_{2g} vibration mode (sp^3 bonding in conjunction with a long-range order) of the nanodiamond prior to and after graphitization with different values of r. As the phonon-confinement model explains [29], the Raman shift peak corresponding to the F_{2g} vibration mode of the nanodiamond is asymmetric with a main peak around 1331 cm^{-1}, and the asymmetry is enhanced as the graphitization temperature increases, since $r'_{C,eff}$ decreases as the temperature increases. In addition, one can find an increase in the peak shift toward lower frequency as the graphitization temperature increases, and the increase in the shift is larger for the nanodiamond with the smaller initial radius as is apparent in figure 5(b). The effect given by variation in the temperature on Raman spectra of the graphitized nanodiamond can be found in variation in the linewidth (full width at half-maximum) of the peak corresponding to the F_{2g} vibration mode. As shown by the broad peak in figure 5(a) and the inset of 5(b), an increase in the graphitization temperature gives rise to an increase in the linewidth, and the increasing behaviour is prominent for the smaller nanodiamond. These behaviours of the variation in the linewidth of the peak corresponding to the F_{2g} vibration mode match well with the experimental results in the literature [4, 12, 13]. By comparing the calculated Raman spectra, one can systematically examine and characterize the degree of graphitization of the nanodiamond under certain graphitization conditions.

References

[1] Choi W B, Cuomo J J, Zhirnov V V, Myers A G and Hren J J 1996 *Appl. Phys. Lett.* **68** 720
[2] Osipov Yu V *et al* 2006 *Carbon* **44** 1225
[3] Greiner N R, Phillips D S, Johnson J D and Volk F 1998 *Nature* **333** 440
[4] Chen J, Deng S Z, Chen J, Yu Z X and Xu N S 1999 *Appl. Phys. Lett.* **74** 3651
[5] Kuznetsov V L *et al* 1994 *Carbon* **32** 873
[6] Alexenskii A E *et al* 1997 *Phys. Solid State* **39** 1007
[7] Butenko Yu V *et al* 2000 *J. Appl. Phys.* **88** 4380
[8] Affoune A M *et al* 2001 *Chem. Phys. Lett.* **348** 17
[9] Campbell I H and Fauchet C M 1986 *Solid State Commun.* **58** 739
[10] Kobashi K, Nishimura J, Kawate Y and Horiuchi T 1988 *Phys. Rev.* B **38** 4067
[11] Shroder R E, Nemanich R J and Glass J T 1990 *Phys. Rev.* B **41** 3738
[12] Yoshikawa M, Mori Y, Obata H, Maegawa M, Katagiri G, Ishida H and Ishitani A 1993 *Appl. Phys. Lett.* **62** 3114
[13] Yoshikawa M, Mori Y, Obata H, Maegawa M, Katagiri G, Ishida H and Ishitani A 1995 *Appl. Phys. Lett.* **67** 694
[14] Nishitani-Gamo M, Ando T, Yamamoto K, Watanabe K, Denning P A, Sayo Y and Sekita M 1997 *Appl. Phys. Lett.* **50** 1530

[15] Solozhenko V L, Turkevich V Z, Kurakevych O O, Crichton W A and Mezouar M 2002 *J. Phys. Chem.* B **106** 6634
[16] Andreev V D 1999 *Phys. Solid State* **41** 627
[17] Wang C, Chen J, Yang G and Xu N 2005 *Angew. Chem. Int. Edn* **44** 7414
[18] Wang C X, Yang Y H, Xu N S and Yang G W 2004 *J. Am. Chem. Soc.* **126** 11303
[19] Bundy F P *et al* 1995 *Nature* **176** 51
[20] Gogotsi Y G *et al* 1996 *Diamond Relat. Mater.* **5** 151
[21] Kraft T and Nickel K G 2000 *J. Mater. Chem.* **10** 671
[22] Gogotsi Y G, Welz S and Ersoy D A 2001 *Nature* **411** 283
[23] Lou Z S *et al* 2003 *J. Am. Chem. Soc.* **125** 9302
[24] Lou Z S *et al* 2003 *Angew. Chem. Int. Edn* **42** 4501
[25] Brodka A, Zerda T W and Burian A 2006 *Diamond Relat. Mater.* **15** 1818
[26] Obraztsova E D, Fujii M, Hayashi S, Kuznetsov V L and Butenko Yu V 1998 *Carbon* **36** 821
[27] Jiang Q and Chen Z P 2006 *Carbon* **44** 79
[28] Gamarnik M Y 1996 *Phys. Rev.* B **54** 2150
[29] Ager J W III, Veirs D K and Rosenblatt G M 1991 *Phys. Rev.* B **43** 6491